Clays and Clay Minerals, Vol. 40, No. 2, 212–229, 1992.

AN ELECTRON OPTICAL INVESTIGATION OF THE ALTERATION OF KAOLINITE TO HALLOYSITE

BALBIR SINGH AND R. J. GILKES

Soil Science and Plant Nutrition, School of Agriculture
The University of Western Australia, Nedlands, W.A., 6009, Australia

Abstract—Parallel-oriented and exceptionally long (>10 μm) tubes of halloysite occur in the pallid zone of a deeply-weathered lateritic profile on granite in southwest Australia.

Transmission electron microscopy and selected-area electron diffraction of ultrathin sections showed that kaolinite plates within pseudomorphs of mica crystals had fractured at irregular intervals along the *a* crystallographic axis to produce laths elongated along the *b* axis. The laths near the edges of the pseudomorphs were less constrained by the pseudomorph and had rolled to produce halloysite tubes. The tubes varied in diameter and degree of roundness. Some tubes were polyhedral rather than cylindrical in cross section. The length and number of planar faces in a tube and the angle between faces varied, exhibiting no consistent pattern.

Tubes in dispersed clay samples showed two types of twinning. In the first type, tubes and associated laths were joined together side by side. In the second type, single tubes bifurcated into two individual tubes. It is proposed that the first type of twinning occurred by folding of adjacent laths that remained joined together while the second type occurred due to exfoliation of a thick lath followed by folding of the exfoliated lath fragments into tubes.

Analytical electron microscopy showed that the chemical compositions of halloysite tubes, laths, and kaolinite plates were similar with the average cation exchange capacity of single tubes being small (4.5 meq/100 g) but higher than values for laths (2.8 meq/100 g) and plates (1.9 meq/100 g).

Key Words—Halloysite, Kaolinite, Mica, Microtomy, Scanning electron microscopy, Transmission electron microscopy.

INTRODUCTION

Halloysite has been reported to form by alteration of feldspars (Anand *et al.*, 1985; Banfield and Eggleton, 1990), biotite (Eswaran and Bin, 1978), and volcanic glass (Kirkman, 1981). Halloysite derived from volcanic glass mostly exhibits a spheroidal crystal morphology whereas the dominant morphology of halloysite derived from crystalline minerals such as feldspars and micas is tubular. Alteration of feldspars and volcanic glass to halloysite must involve a solution and/or an amorphous phase because the structures of these parent minerals are completely different from that of halloysite. Consequently, topotaxial or epitaxial alteration is not possible and there is no consistent orientation of the secondary mineral relative to the parent mineral (Gilkes *et al.*, 1986). The structure and composition of micas on the other hand are closely related to these properties of kaolin-group minerals and oriented growth of secondary kaolinite with crystallographic axes parallel to those of the parent mica is common (i.e., topotaxial alteration) (Gilkes and Suddhiprakarn, 1979; Ahn and Peacor, 1987; Banfield and Eggleton, 1988). However, the alteration of platy mica to tubular halloysite cannot occur by simple topotactic alteration. Hope and Kittrick (1964) demonstrated that thin plates of kaolinite can roll so that kaolinite that had formed from mica by topotactic alteration could subsequently form tubes. Dixon and McKee (1974) observed that some cross sections of halloysite tubes consisted of planar regions resembling kaolinite crystals and suggested that growth had occurred on basal faces subsequent to folding of thin particles. The formation of tubular halloysite by weathering of mica is, however, generally considered to be a result of crystallization from solution rather than topotactic alteration of mica (Giese, 1988; Dixon, 1989). Consequently, explanations for the observed morphological features of tubular halloysite, such as planar faces, twinning of tubes and split tubes, are based on this mode of formation, i.e., from solution (Bates *et al.*, 1950; Kirkman, 1981). The validity of these explanations has recently been questioned by Bailey (1989). In this paper we report on the development of parallel-oriented halloysite tubes and laths by a process of deformation of platy kaolinite pseudomorphs after mica rather than by crystal growth from solution.

There is some inconsistency in the terminology and criteria used to distinguish halloysite from kaolinite (Churchman and Gilkes, 1989). In this study the term kaolin is used to refer to kaolinite and halloysite collectively. Crystals with a platy morphology and kaolin chemical composition are considered to be kaolinite and those with a cylindrical morphology and of the same composition to be halloysite. The term pseudomorph is used to refer to an aggregate of crystals of

secondary mineral(s) that has originated from a single crystal of mica and that has approximately retained its external form.

MATERIALS AND METHODS

A 15 × 15 × 15 cm^3 block of pallid zone material was excavated, with minimum disturbance, from about 5 m depth in a laterite profile developed from granitic rocks. The profile is exposed in a railway cutting at Merredin, 265 km east of Perth, Western Australia. The profile exhibits a sequence of zones typical of *in situ* deeply-weathered lateritic profiles in the region (Gilkes *et al.*, 1973). The sample was taken from the pallid zone, which is a product of extreme chemical weathering and leaching. Abundant quartz veins were preserved in the profile, demonstrating that at least on a macroscopic scale the pallid zone had developed by *in situ* isovolumetric chemical weathering (Millot, 1970).

A portion of the sample was impregnated with epoxy resin and polished thin sections mounted on glass slides were made for optical microscopy and scanning electron microscopy (SEM) using back-scattered electrons (BSE). The BSE images provide information on compositional variations and were used to assist the optical microscope analysis.

Freshly exposed fracture surfaces of the sample were investigated by SEM using a Philips SEM 505 instrument fitted with a back-scattered electron detector and energy dispersive X-ray analyzer (EDX). Specimens of about one cubic centimeter volume were mounted on aluminum stubs and then coated with carbon and subsequently with a 50 Å-thick layer of gold in a vacuum evaporator. Samples for transmission electron microscopy (TEM) examination were prepared in two ways. A dilute suspension of the sample was prepared in distilled water by gently shaking the crushed bulk sample. Complete dispersion of the sample was avoided so as to enable the investigation of the morphology and form of association of halloysite crystals in natural aggregates, and especially pseudomorphs. The <20-μm fraction was separated from the bulk suspension and drops were placed on carbon films with a micropipette. The drops were dried under cover at room temperature. For some samples a gold internal standard was evaporated onto the grids at an angle of 60° with the grid to calibrate the selected area electron diffraction (SAED) patterns and to provide a shadow for the measurement of particle thickness.

To investigate the internal morphology of the pseudomorphs, ultrathin sections were prepared by microtomy. A suspension containing 5–20 μm particles was settled in a flat-bottomed plastic tray and dried at 45°C. The dried sample was vacuum-impregnated with Spurr's resin (Spurr, 1969) and ultrathin sections were cut with a diamond knife using a Reichert-Jung microtome. The ultrathin sections were floated on water, collected on 400-mesh copper grids and coated with a thin layer of carbon. The ultrathin sections and the samples prepared from suspension were investigated using a Philips 430 analytical transmission electron microscope (AEM) operated at 300 kV. Some dispersed samples were also studied by scanning transmission electron microscopy (STEM) using a JEOL 2000FX instrument operated at 100 kV to obtain high-resolution micrographs of the surface morphology of the halloysite crystals.

X-ray diffraction (XRD) patterns of the whole material and the clay fraction were obtained using Cu$K\alpha$ radiation with a computer-controlled Philips vertical diffractometer and graphite diffracted beam monochromator. The digital XRD patterns were interpreted with the aid of XPAS analytical software which enabled rapid calculation of very accurate crystallographic parameters. The formamide intercalation test was used to distinguish halloysite from kaolinite in the bulk sample (Churchman *et al.*, 1984).

RESULTS AND DISCUSSION

Morphology

The pallid zone sample exhibited a typical highly porous nature, white color and preservation of rock fabric (McCrea *et al.*, 1990). Optical micrographs and BSE images of the thin section (Figure 1) show the excellent preservation of the granitic rock fabric with pseudomorphs after primary grains of mica (1), quartz (2), abundant large voids (3), and elongated pores (4). The abundance of voids is due to removal by weathering of a large proportion of the rock (i.e., the alkali and alkali earth components and some Si). This has resulted in residuum of a much lower bulk density than the parent rock. Vermicular kaolin pseudomorphs after mica and the coarse size of quartz grains indicate that the parent material was a micaceous granitic rock, which is of common occurrence in the region (Williams, 1975).

Low-magnification SEM photos of regions of fracture surfaces (Figure 2) show features consistent with those observed in the thin sections. The fabric of the parent material is preserved with high fidelity in the weathered material. Vermicular pseudomorphs after mica (1), bundles of tubes (2), and large voids (3), are present. XRD analysis of the bulk material indicates that it consists mainly of kaolin minerals and quartz (Figure 3A). Therefore, the tubular and platy morphologies observed in the SEM image are probably indicative of halloysite and kaolinite, respectively. The EDX spectra for both morphologies show the major constituents to be Al and Si and are typical of spectra of kaolin minerals (Figure 3B). The stacks of plates are probably kaolinite pseudomorphs after the mica that is a common primary mineral in the parent rock. Pseudomorphs after primary minerals are a common feature of soils developed by *in situ* chemical weathering

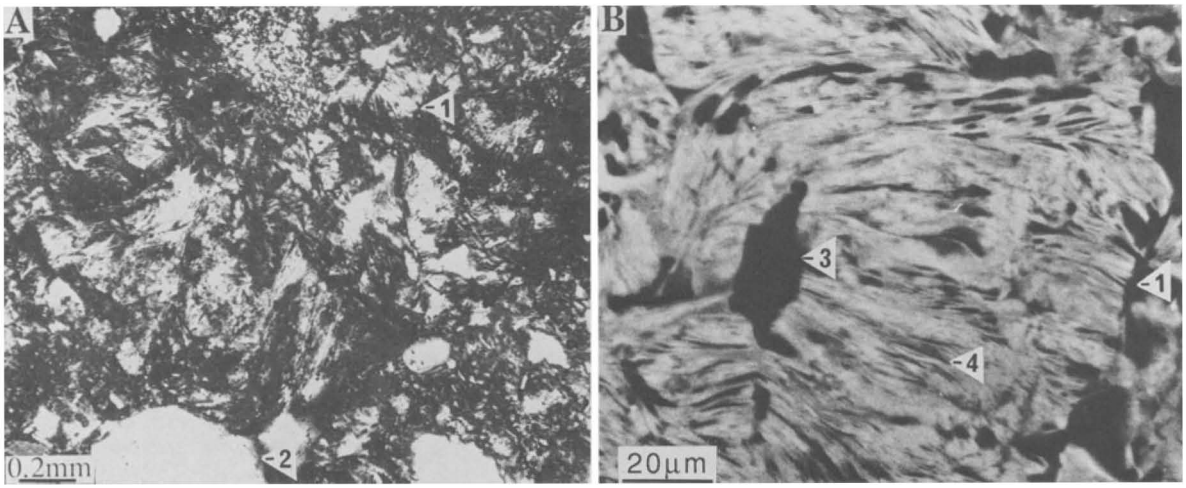

Figure 1. Optical (A) and back scattered electron (B) micrographs of a thin section of resin-impregnated bulk material showing kaolinite/halloysite pseudomorphs of mica crystals (1), quartz grains (2), voids (3), and elongate pores (4).

(Keller, 1978). Many studies of the weathering of biotite and muscovite have reported the oriented growth of kaolinite to form pseudomorphs (Gilkes and Suddhiprakarn, 1979; Ahn and Peacor, 1987; Banfield and Eggleton, 1988, 1990). The bundles of tubes (Figure 4A) show clear boundaries and appear to be more densely packed than halloysite masses that are considered to have crystallized from solution (Keller, 1978; Banfield and Eggleton, 1990). Tubes occur in close association with plates from which they may have formed by rolling (Figures 4B–4D). End views of the tubes show a rolled configuration and most of the tubes are not tapered. Halloysite tubes that are considered to have crystallized from solution often have tapered ends (Keller, 1978; Kirkman, 1981).

Halloysite is a common weathering product of feldspars and biotite in granitic rocks, and usually occurs as randomly oriented felted masses or as radiating spherical aggregates (Eswaran and Bin, 1978; Keller, 1978; Kirkman, 1981; Anand *et al.*, 1985). Radiating spherical aggregates of halloysite are believed to indicate that halloysite has crystallized from solution in a void (Banfield and Eggleton, 1990). Felted planar masses may be formed of halloysite that crystallized

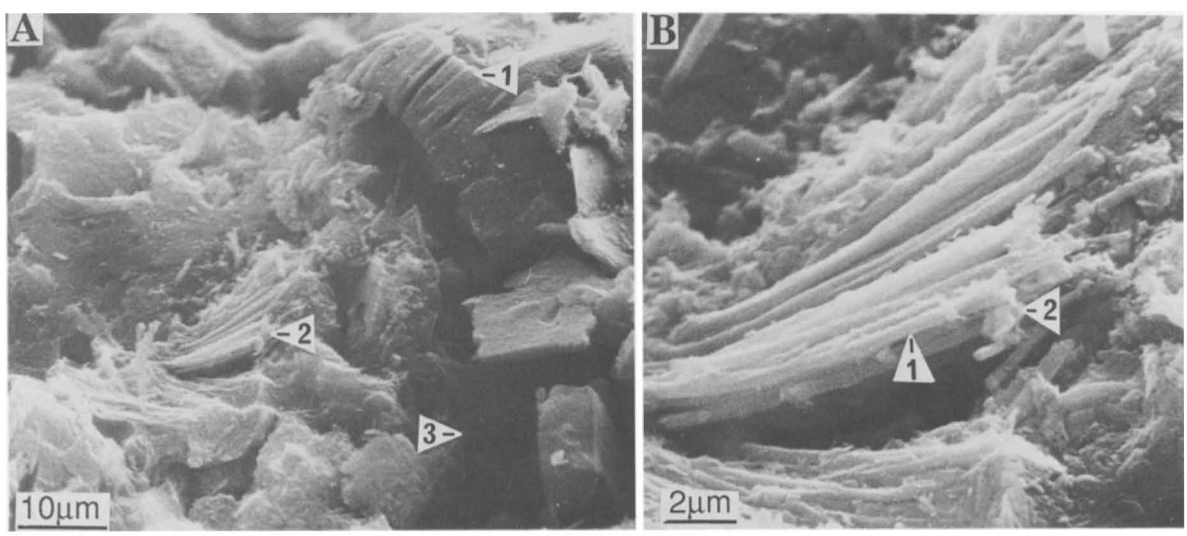

Figure 2. Scanning electron micrographs of a fracture surface of the bulk material. (A) Pseudomorphs after primary mica grains (1), a bundle of tubes (2), and large voids and pores (3) are present and are indicative of the granitic fabric of the parent rock. (B) High-magnification view of a bundle of tubes shown in A. The tubes (1) are curved, show a near-parallel orientation and are more than 10 μm long. Some fine, platy anhedral material (2) is attached to the walls of tubes.

https://doi.org/10.1346/CCMN.1992.0400211 Published online by Cambridge University Press

in the confined space provided by planar voids (McCrea *et al.*, 1990). In contrast to these commonly observed morphologies, some halloysite crystals in this material exhibit an unusually high degree of parallel orientation and are much longer (~10×) than is normal for halloysite in laterite pallid-zone materials (McCrea *et al.*, 1990). It is probable that this association of a parallel orientation and an extreme length have a common origin that is the major topic of investigation of this paper.

Souza Santos (1966) reported the occurrence of a tubular kaolin material from Brazil with a macroscopic fibrous appearance that was believed to be due to parallel orientation of the constituent halloysite crystals. This material occurred in layers within cracks in weathered granite and may have adopted the parallel orientation due to restriction by the geometry of the cracks or to flow in the cracks of suspensions carrying halloysite crystals. Bundles of halloysite tubes in the present specimen occur uniformly throughout the body of the weathered material and the longitudinal direction of the bundles exhibits a random orientation within the sample. Bundles are mostly isolated from each other and show well-defined boundaries (Figure 4), demonstrating that macroscopic flow conditions are not responsible for the parallel orientation of these halloysite tubes. Halloysite tubes crystallized from solution can also achieve some degree of parallel orientation (Keller, 1978), but they mostly radiate outwards from the substrate and are less densely packed. Micas exhibit a perfect cleavage along (001) and commonly exfoliate along this plane in the initial stages of weathering thereby creating an array of parallel slits (Gilkes and Suddhiprakarn, 1979). Such parallel slits provide an environment that would generate a planar (two dimensional) mat of halloysite tubes but would not lead to a high degree of orientation of tubes in three dimensions.

Some bundles (Figure 5A) seem to consist of flat-surfaced laths rather than tubes, and these laths are joined together to produce a raft-like appearance. This morphology suggests that the parallel laths may have originated by parallel fracturing of a larger plate at regular intervals. A graphic representation of the fracture of plates into laths is shown in Figure 5B. The direction of fracture might be crystallographically controlled. The parallel laths may subsequently fold or roll to form an array of parallel tubes. This mechanism for the development of oriented tubes from kaolinite plates was first proposed by Brindley and Comer (1956).

Internal morphology of the pseudomorphs

SEM indicates that bundles of parallel-oriented halloysite tubes might have formed by rolling/folding of kaolinite plates and laths. If that is the case then all stages of this transformation of plates into laths and subsequent rolling/folding of laths might be expected to be present in the materials obtained from this soil

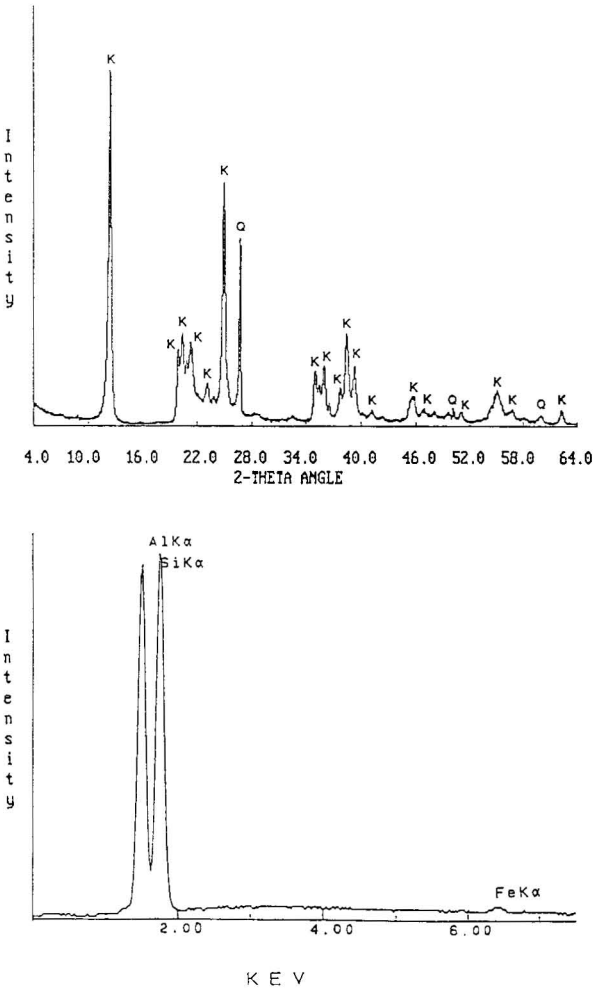

Figure 3. (A) Powder XRD pattern of bulk material showing it to be a mixture of a 7 Å kaolin group mineral and quartz, and (B) an EDX X-ray spectrum from SEM that is representative of spectra obtained for stacks of plates and bundles of tubes similar to those shown in Figure 2.

profile. Fractured surfaces examined by SEM may not represent the bulk of the material as fracturing exposes the exterior surfaces of aggregates rather than the interior surfaces. Therefore, the SEM study of fracture surfaces may have been inadvertently restricted to advanced stages of the transformation where aggregates of halloysite tubes are more loosely packed and would part (fracture) most easily. In order to investigate the internal morphology of aggregates and, in particular, pseudomorphs after mica that might include early stages of the proposed transformation, ultrathin sections of the 5–20 μm size fraction of the sample were prepared. The <5-μm fraction was excluded so that natural aggregates/pseudomorphs could be distinguished as isolated regions of high particle concentration with clear boundaries. Particles larger than 20 μm were removed to exclude quartz grains that could have damaged the

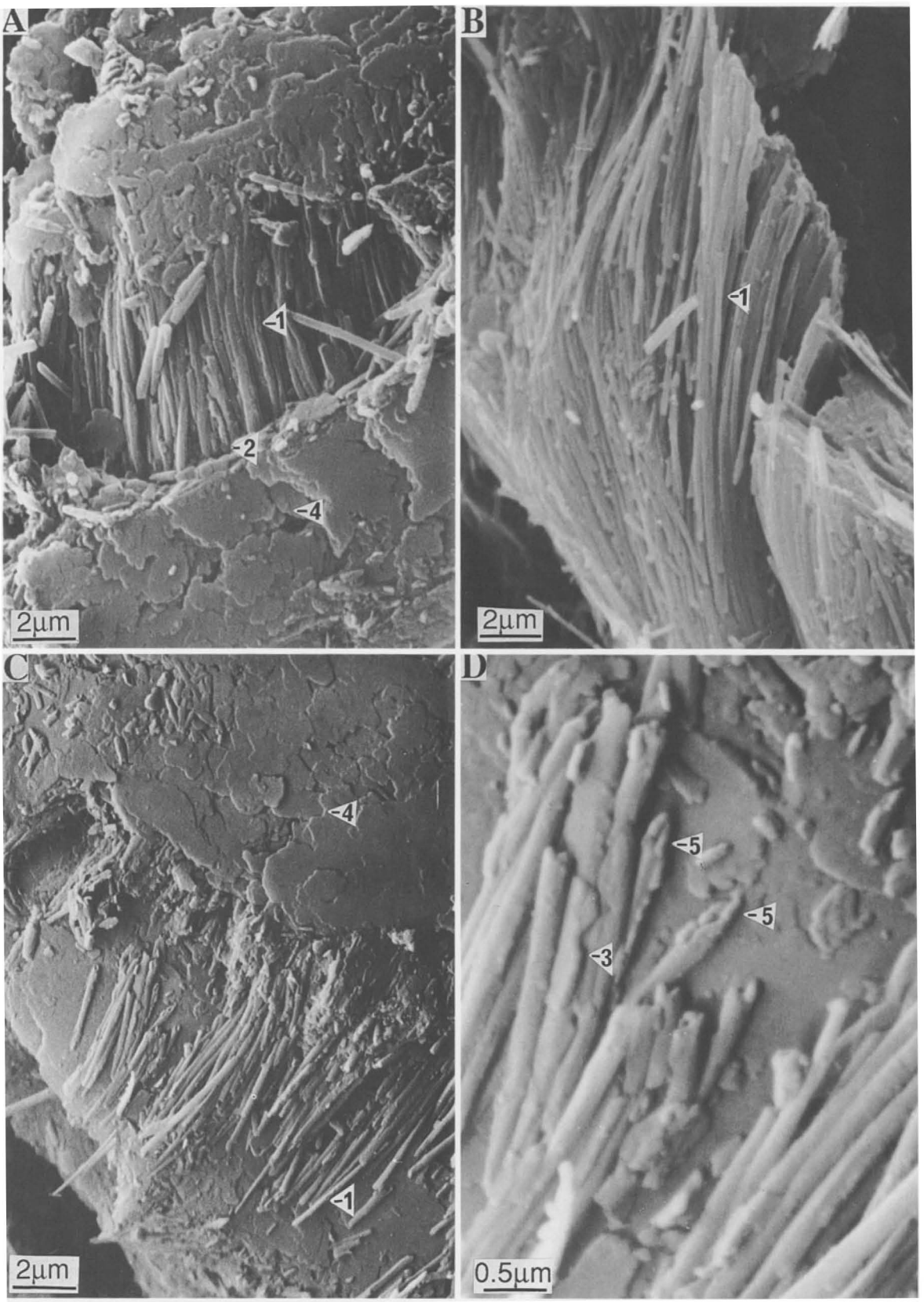

https://doi.org/10.1346/CCMN.1992.0400211 Published online by Cambridge University Press

diamond knife. This technique allowed the natural association of the particles within the pseudomorphs to be viewed at high resolution.

A micrograph of a section across the basal plane of a mica pseudomorph is shown in Figure 6A. Longitudinal units comprising much of the area of the micrograph represent a side view of stacks of kaolinite plates that are about 0.2 μm thick and 10 μm wide. Polygonal and circular features on the right-hand side of the micrograph represent the cross-sectional view of halloysite tubes of diameters ranging from 0.2 to 0.4 μm (Figure 6E). The plates exhibit a range of morphologies. At location (1) plates are straight and are mostly unfractured (Figure 6B is a enlarged view of this region). At location (2) plates show thin lines of fracture across plates (Figure 6C) that widen to produce discrete regions or crystallites (Figure 6D). Scours made by the diamond knife on the sample and resin represent the direction of the advancing cut (5 in Figure 6A). In the regions where the pieces of fractured plates are sufficiently separated, the vacant space is filled with impregnating resin, which suggests that the fractures may be an original feature of this material. It is, however, also possible that these fractures are caused by the impact of the diamond knife, as minerals may fracture along crystallographic directions determined by stress/strain relationships (Towe and Hamilton, 1968), and resin may move by plastic flow during sectioning. In many pseudomorphs, halloysite tubes and partially-folded laths occurred in a row next to the end of a wavy and deformed plate (Figure 7), suggesting that the row of tubes originated from plates by rolling after periodic fracture. In the samples prepared from suspensions, laths longitudinally fractured and folded to produce tubes were present (Figure 8), and tubes and laths in the partially dispersed bundles (Figure 9) occurred in near parallel orientation. All the halloysite tubes and laths in the bundles that were analyzed by selected area electron diffraction were elongated along the *b* axis, which suggests a common origin for these two components. The laths often exhibited regular hexagonal terminations (Figure 9B) often with a face normal to the axis of elongation. These observations suggest that parallel-oriented halloysite tubes are derived from plates of kaolinite.

SAED was employed to identify the crystallographic orientation of the fracture lines within the pseudomorphs. Systematic tilting of the pseudomorphs to obtain the orientation necessary for symmetrical diffraction patterns was not possible due to the small size of the fractured sections and to the material being very sensitive to beam damage. Therefore, to avoid a long exposure to the electron beam associated with tilting of the specimens, pseudomorphs sectioned through a major plane and showing identifiable morphological features were chosen for SAED analysis. A micrograph and its correctly oriented SAED pattern for such a cross section are shown in Figure 10. The SAED pattern indicates that the pseudomorph is sectioned approximately perpendicular to the *b* axis so that the *b* axis is approximately parallel to the electron beam. The elongated features seen in the micrograph therefore represent an *ac* section of the kaolinite plates. The plates have been fractured at irregular intervals along the *a* axis to form laths and the laths have been separated in some regions. The width of the laths (*a* direction) ranges from 0.1 to 0.5 μm with an average size of 0.2 μm. The thickness of the laths (*c* direction) varies from 0.02 to 0.1 μm. The pseudomorphs were too small to be relocated in multiple serial sections so that the length of laths in the *b* direction could not be determined.

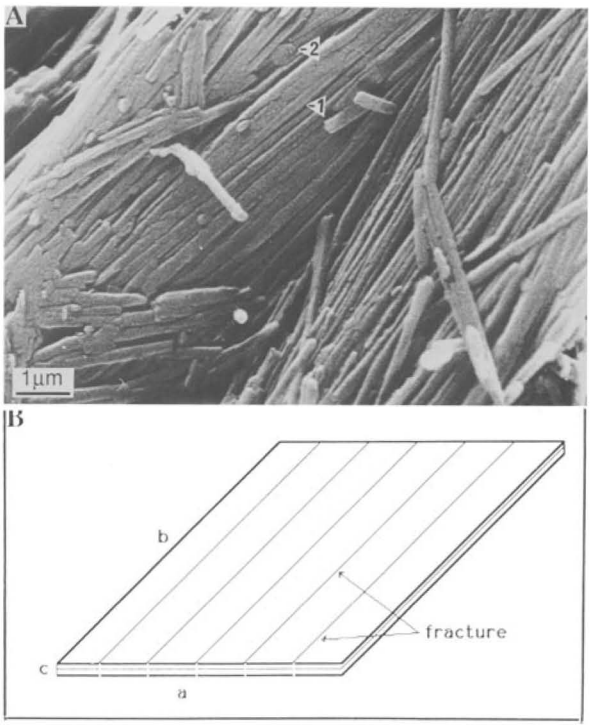

Figure 5. (A) Scanning electron micrograph of a fracture surface showing laths and tubes. The laths (1) are aligned to produce a composite raft-like appearance. Some anhedral platy particles (2) are also present. (B) A graphic representation of a possible mechanism for the fracture of a plate into laths.

←

Figure 4. Scanning electron micrographs of regions of fracture surfaces showing bundles of parallel tubes (1) with distinct boundaries (2), possible laths (3), and kaolinite plates exhibiting characteristic 120° angles (4). A magnified view of a part of C is shown in D. The rolled configuration of plates to form tubes (5) is clearly seen.

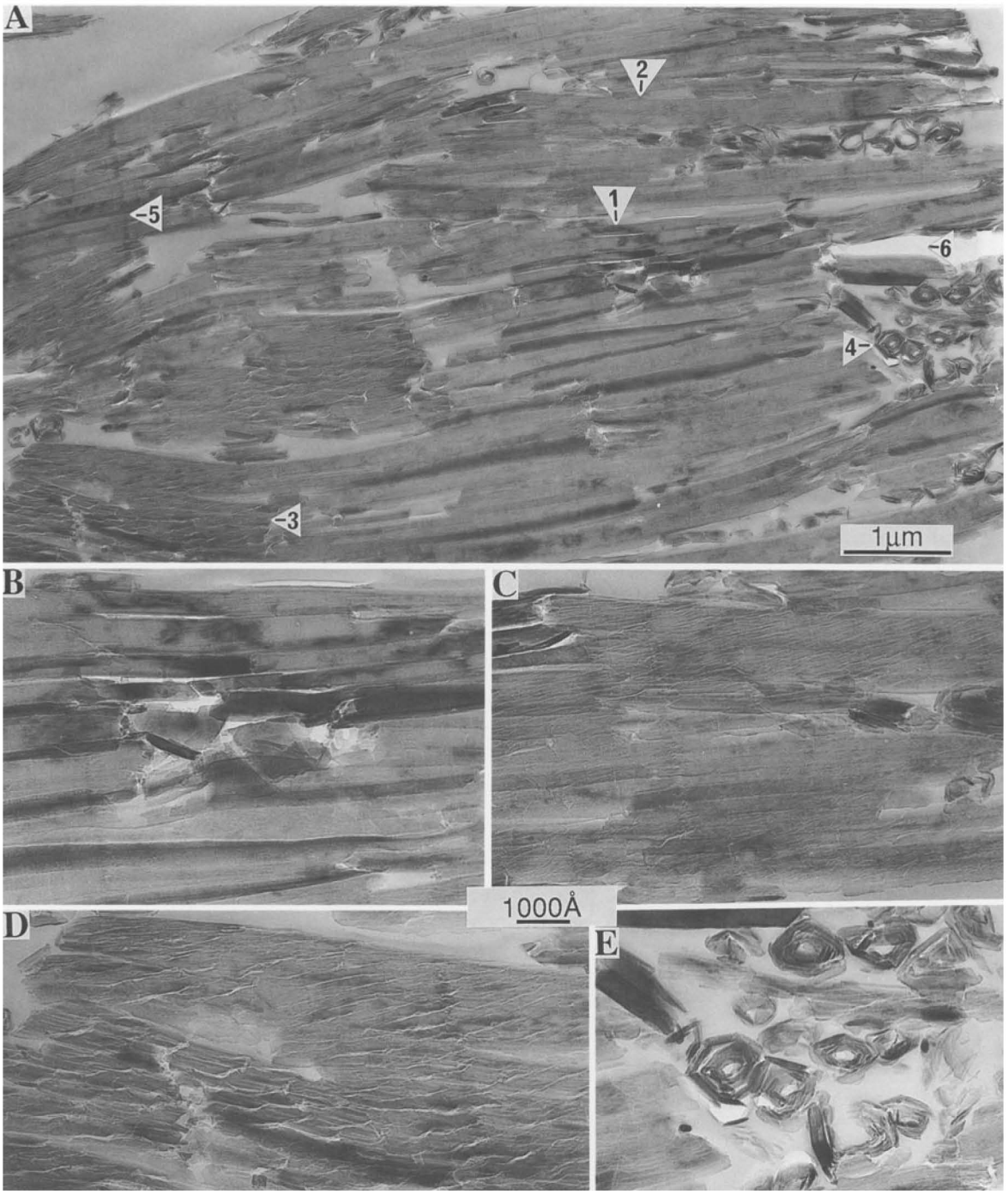

Figure 6. (A) Transmission electron micrograph of an ultrathin section of a pseudomorph after mica. B, C, D and E are photographic magnifications of the regions in A marked 1, 2, 3 and 4, respectively. The longitudinal features occupying much of the area are sections of stacks of kaolinite plates. The plates show a range of morphological states: unfractured (1), fractured but attached (2), fractured and separated (3), fractured and partly or completely rolled/folded to form tubes (4). Scours made by the diamond knife are present (5). The regions not filled with resin (6) are recognized by their brighter background.

The fracture line across the plates makes an angle of approximately 55° with the *c* axis. Since the fracture line is not parallel to the *c* axis, a ragged or diffuse edge to particles would be seen in TEM images of individual kaolinite crystals deposited from suspension onto carbon films.

The evidence presented here indicates that halloysite tubes have formed by rolling/folding of kaolinite laths

https://doi.org/10.1346/CCMN.1992.0400211 Published online by Cambridge University Press

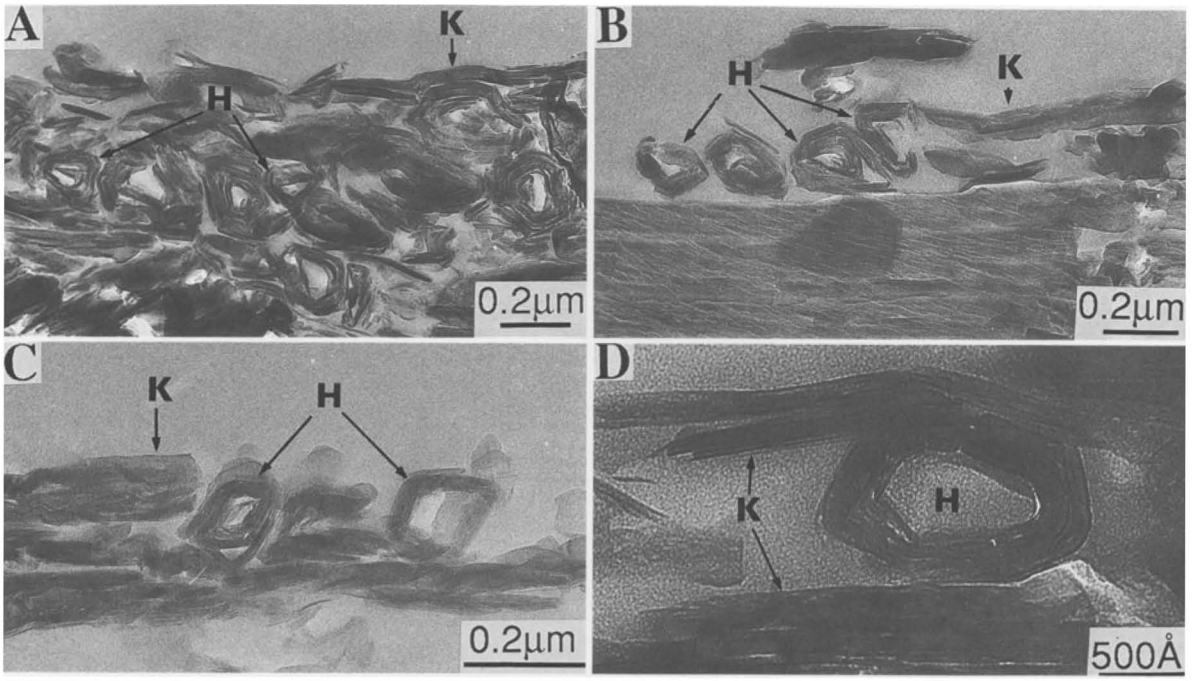

Figure 7. Transmission electron micrograph showing halloysite (H) associated with kaolinite (K). (A) Halloysite tubes in parallel packing are flanked by wavy and discontinuous kaolinite plates. (B, C) A row of halloysite tubes at the end of a plate. (D) A halloysite tube in contact with and confined by kaolinite plates.

that have been derived by regular fragmentation of large kaolinite plates in pseudomorphs of mica crystals. A similar transformation of kaolinite to halloysite has been reported by Robertson and Eggleton (1991). It seems that kaolinite plates may be fractured by unbalanced forces in the structure that subsequently cause them to curve/fold around a preferred crystallographic direction (i.e., the *b* axis). The unbalanced forces in platy kaolin minerals can be due to the unequal dimensions of the tetrahedral and octahedral sheets (Bates *et al.*, 1950; Bailey, 1989) or to contraction of the outer hydroxyl plane (i.e., the hydroxyl plane facing interlayer space) of the octahedral sheet (Radoslovich, 1963b). As the laths in these pseudomorphs are initially confined within slit-shaped voids in pseudomorphs they cannot curve uniformly in this restricted volume to form tubes as would be possible for isolated (unconfined) laths. Instead, once the laths have formed by fracturing of sheets they tend to curve into arcuate shapes first, and only when exfoliation of layers of the pseudomorphs provides sufficient space does complete rolling/folding of laths occur. A graphic representation of the phenomenon is shown in Figure 11.

A micrograph of a pseudomorph exhibiting an advanced stage of the transformation sequence described above is shown in Figure 12 with the direction of sectioning being across the axis of elongation of the laths and tubes. Fractured plates similar to those present at the initial stages of transformation (cf, Figure 6) are present in parts of the pseudomorph. Most of the pseudomorph consists of a mixture of laths, partially rolled/folded laths, and tubes. The region where most of the plates have altered to tubes is very porous suggesting that rolling/folding of laths requires adequate free space and could not occur in the more confined region of this pseudomorph. Some tubes appear to be joined together by residual fragments of the former plate/lath that adhere to the outer walls of the tubes (Figure 13). The tubes range in diameter from 0.1 to 0.5 μm. The larger tubes have thick planar outer walls and appear to be folded rather than rolled. The inner part of the larger tubes is more uniformly curved. The shape of tube cross sections varies substantially and includes nearly circular, elliptical, polygonal, and only partially rolled (arc-like) forms. Evidence for the tubes being formed by rolling of plates/laths is provided by those particles that are only partially rolled and where the residual plate extends from the roll (Figures 6E, 13). Similar tube cross sections suggestive of folded kaolinite were also observed by Dixon and McKee (1974). The other cross-sectional features of halloysite in this specimen (viz, planar faces, width of faces, shape of cross sections) are also consistent with those described by Dixon and McKee (1974).

Planar faces of halloysite tubes

Planar faces are present mainly on large tubes with diameters of 0.2 to 0.5 μm. The number of faces on

https://doi.org/10.1346/CCMN.1992.0400211 Published online by Cambridge University Press

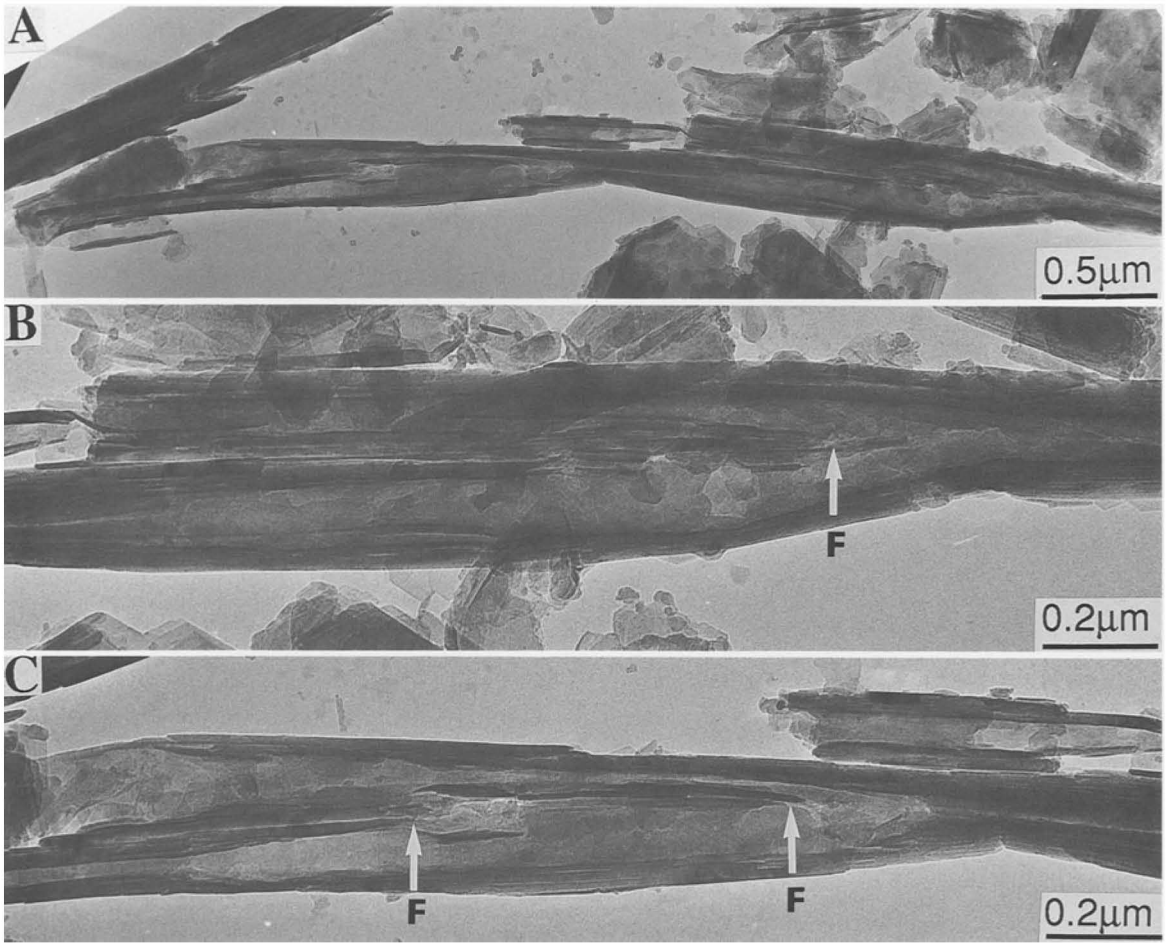

Figure 8. Transmission electron micrograph showing twinned halloysite tube/lath assemblages produced by fracture of a single lath/tube. B and C are enlarged views of A. The fractures (F) are indicated by white arrows. The regions to the right side of the arrows are unfractured as indicated by the smooth contrast. On the left side the regions have fractured and folded.

each tube, their width and the angle between faces vary considerably. The width of planar faces ranges from 0.1 to 0.5 μm, which is of the same order as the width of laths. The joint between planar faces (i.e., the "hinge") shows discontinuous separations. In some crystals planar components extend outwards from the tube (Figures 12, 13). These observations suggest that the planar components represent laths or parts of laths which have not curved/bent completely. Laths with no apparent curvature, uniformly folded/curved laths, and intermediate morphologies are common and are randomly intermixed in micron-sized regions of thin sections. This complexity demonstrates that those factors responsible for rolling vary over small distances within a single pseudomorph. The balance between the forces that promote/prevent rolling may also vary within a single lath causing it to present curved and planar surfaces along its length (Figure 14). Laths showing varying degrees of curvature were commonly observed in dispersed samples.

Planar faces on tubular and spheroidal halloysite crystals have been described by other workers (Chukhrov and Zvyagin, 1966; Dixon and McKee, 1974; Kirkman, 1981). The explanations offered for the planar faces are "flattening" due to dehydration (Bailey, 1989), polygonization (Kirkman, 1981), and radial growth of tubes terminating at planar (001) faces (Chukhrov and Zvyagin, 1966). There are strong arguments against each proposal (Bailey, 1989). Most workers have considered curved halloysite tubes to be an original form due to crystallization from solution rather than a form produced by rolling of platy kaolinite as is proposed here. In view of the evidence presented here for plates fracturing and folding to form tubes, and with every intermediate stage being represented in a single micrograph, the present explanation must also be considered.

Morphology of the dispersed crystals

The detailed morphology of particles in the <10-μm fraction was investigated by TEM. Halloysite crystals

https://doi.org/10.1346/CCMN.1992.0400211 Published online by Cambridge University Press

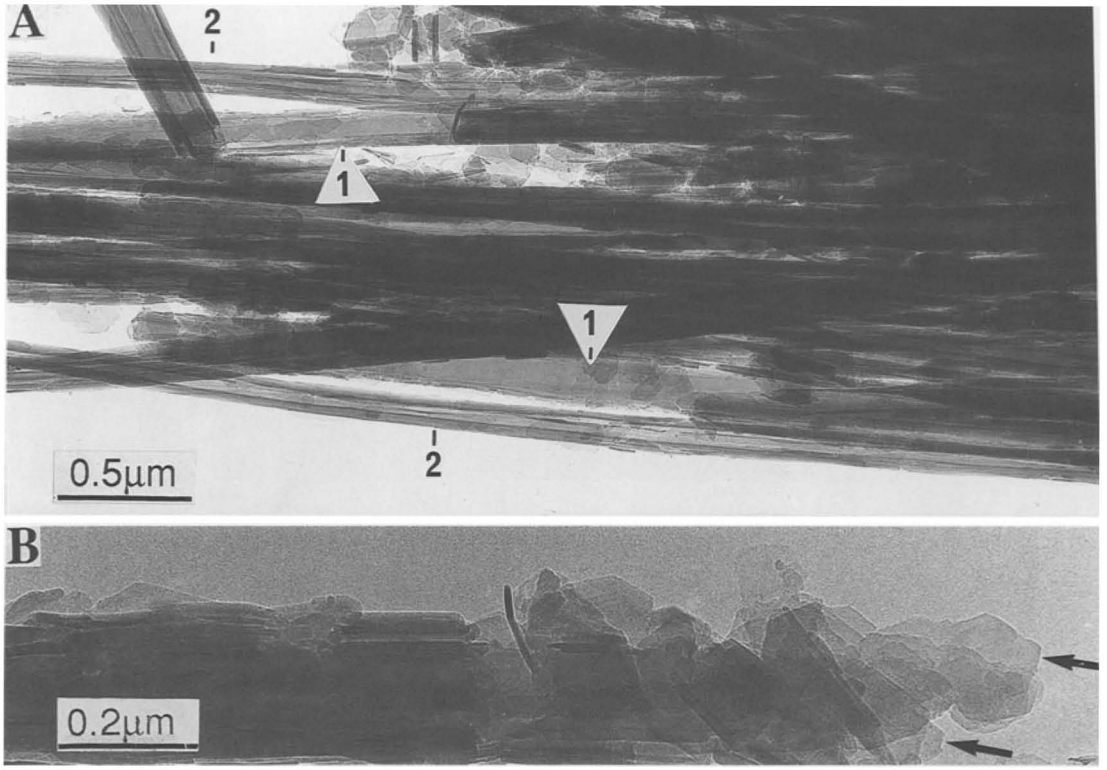

Figure 9. (A) Transmission electron micrograph of a bundle of laths (1) and tubes (2) in a dispersed sample. Laths and tubes are in subparallel orientation in the bundle. (B) Enlarged view of a lath showing regular hexagonal features (indicated by arrows). The terminating face is approximately normal to the axis of elongation.

occurred in a variety of shapes, sizes, and arrangements (Figure 14). Most of the halloysite crystals were between 0.05 to 0.5 μm in diameter and 0.5 to 2 μm in length, with only a few very long (10–20 μm) and parallel-oriented crystals, which might seem to be inconsistent with the observations made by SEM and TEM on sectioned samples and described above. The longer crystals that are so evident in SEM micrographs may have been broken during sample preparation even though the clay samples used for TEM were prepared by gentle crushing and dispersion. Almost all tubes showed jagged ends and partly fractured tubes were present. The dispersed sample also contained about 0.12-μm thick euhedral to subhedral hexagonal kaolinite crystals (Figure 15). These appear to be complex twinned crystals and resemble the kaolinite crystals described by many other workers (e.g., Bates, 1971).

We believe that the type of transformation of kaolinite to halloysite observed in this study and the consequent occurrence of long and parallel-oriented crystals may be of widespread occurrence in soils. It is undetected when only clay fractions (<2 μm) are observed by TEM because most clay in the <2-μm fraction is derived from the matrix rather than from pseudomorphs of mica. For instance, the halloysite described by Ross *et al.* (1983) may well have formed by this mechanism. The halloysite tubes shown in their Figure 6 were about 10 μm long and were joined together side by side. The deep sub-soil profile investigated by these workers was developed by *in situ* weathering of a rock that contained biotite so that kaolinite pseudomorphs after mica could have been present as is the case in the present study.

Twinning of halloysite crystals

Most of the halloysite crystals existed as individual particles. Some crystals, however, exhibited bifurcation or twinning, two types of which were common. In the first type the tubes were joined together side by side (Figures 8, 16A). Tubes of this type (Type 1) may have formed by folding of adjacent laths within a fractured plate, part of which remained joined. In the second type (Type 2) thick, single laths cleaved along (001) into two laths and each lath rolled into a tube (Figure 16B). The two mechanisms are thus simply a result of cleavage of kaolin plates in directions that are approximately perpendicular (Type 1) or parallel (Type 2) to the basal cleavage of the parent mica crystal. Bates *et al.* (1950) observed semicircular indentations of the surfaces of tubes and believed that they represented the place where an intergrown tube had broken away.

https://doi.org/10.1346/CCMN.1992.0400211 Published online by Cambridge University Press

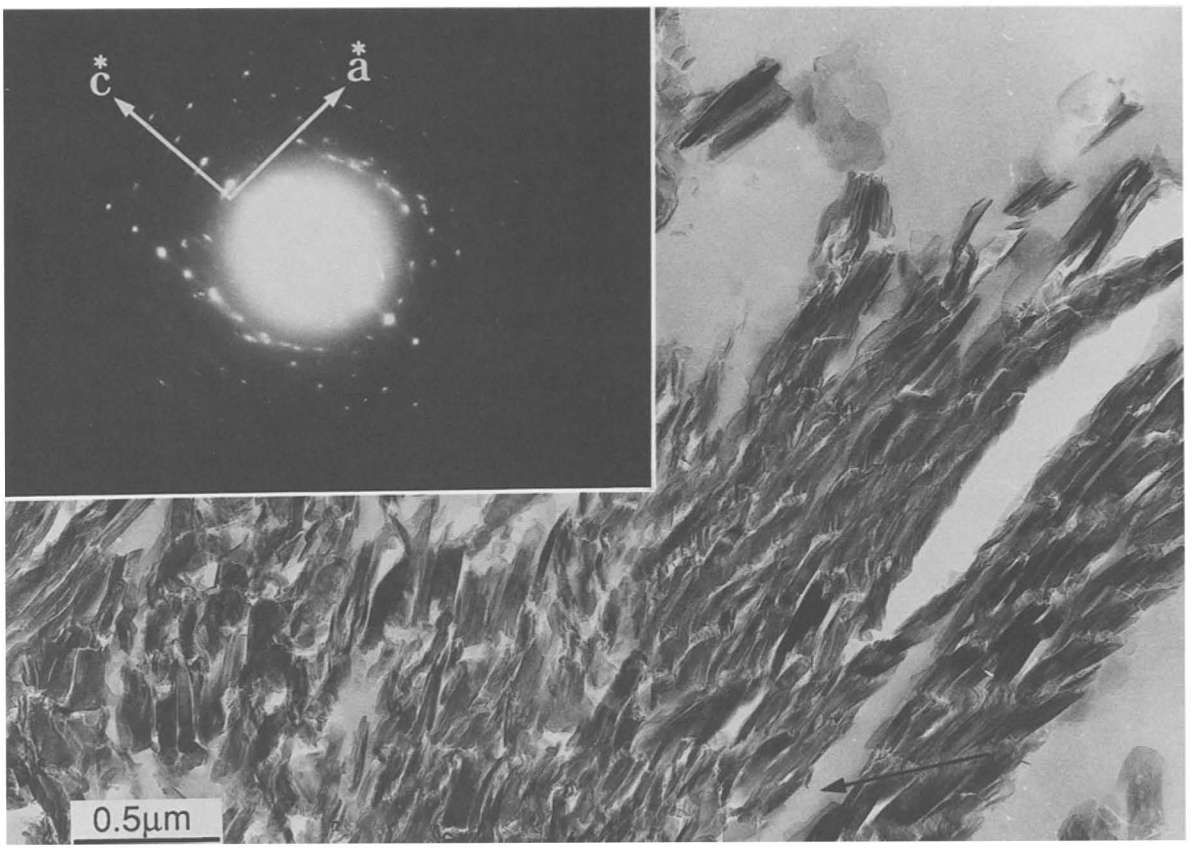

Figure 10. Transmission electron micrograph of a region of a pseudomorph consisting of kaolinite and the corresponding correctly oriented SAED pattern. The SAED pattern demonstrates that the pseudomorph was sectioned approximately parallel to the (010) plane and that the fracture line (parallel to the black arrow on the micrograph) makes an angle of approximately 55° with the *c* axis.

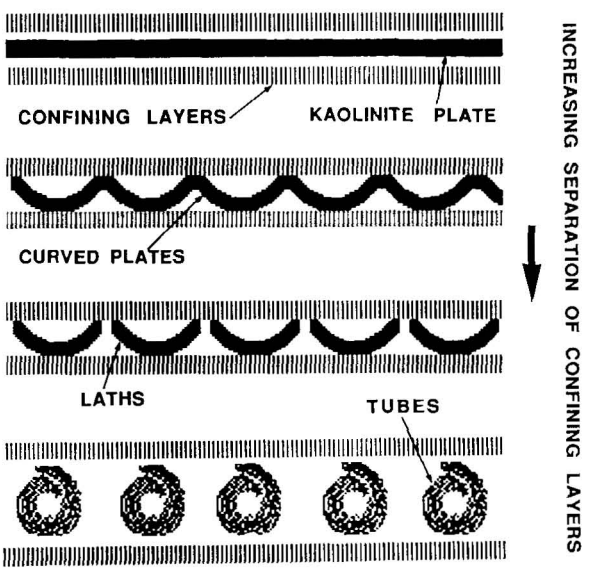

Figure 11. A graphic representation of the transformation of a confined kaolinite plate in a pseudomorph to curved laths and tubes as the separation of confining layers increases.

Such indentations were not observed in the present study.

Unit cell parameters

The unit cell parameters of the various types of halloysite tubes and associated kaolinite plates were determined from SAED patterns calibrated with a gold internal standard. A typical SAED pattern of a gold-shadowed halloysite crystal is shown in Figure 17. The pattern is characteristic of tubular crystals (i.e., resembles an XRD rotation pattern) with the a^* and c^* axes on a common axis perpendicular to the b^* axis, which is the axis of elongation. The orientation of hexagonal plates on the crystal surface (Figure 17) as indicated by their shadows is consistent with the symmetry of the SAED pattern suggesting that these hexagonal terminations (Figures 9B, 17) are features of the main crystal, and thus the face normal to the axis of elongation is the (010) face. The c^*-axis periodicity is approximately 14 Å so that the pattern can be indexed on the basis of a two-layer structure. All the crystals analyzed by SAED (~50) were elongated along the *b*

https://doi.org/10.1346/CCMN.1992.0400211 Published online by Cambridge University Press

Figure 12. Transmission electron micrograph of a pseudomorph showing an advanced stage in the formation of laths and halloysite tubes. Fractured plates (1) (as in Figure 6), laths (2) and tubes (3) are present. The tubes and laths (4) in the highly porous region have retained a degree of *b*-axis parallelism with the fractured plates (1).

axis and showed this two-layer periodicity. Robertson and Eggleton (1991) reported halloysite elongated along the *a* axis. Their interpretation may be questioned as it was based on a streaky SAED pattern obtained with the electron beam approximately parallel to the tube axis. The axis of elongation is best determined from SAED patterns obtained with the tube axis normal to the beam (as is the case with tubes resting on a carbon film). This allows the direct determination of the periodicity of the structure in the direction of the tube axis. Halloysites elongated along the *a* axis are extremely rare (Bailey, 1989). The two-layer structure of halloysite has been consistently observed by various workers (Honjo *et al.*, 1954; Chukhrov and Zvyagin, 1966; Kohyama *et al.*, 1978; Noro, 1986) and, therefore, may be considered a characteristic of tubular halloysites. The unit cell parameters measured from SAED patterns of halloysite were a = 5.14 Å, b = 8.92 Å and c = 14.4 Å. These cell parameters are similar to those reported by other workers (e.g., Honjo *et al.*, 1954; Kohyama *et al.*, 1978). The morphology and *b* dimension of halloysite are believed to depend on the iron content of the structure (Radoslovich, 1963a; Bailey, 1989). The *b* dimension and iron content of this specimen determined by AEM (Table 1) are consistent with values for the tubular halloysite described by Noro (1986). The unit cell parameters and composition of this specimen resemble values for other tubular halloysites, despite the unusual length and parallel orientation of the tubes.

Elemental composition of the morphologically-distinct crystals

Variations in the morphology of halloysite have been considered to be a consequence of cation substitutions in the tetrahedral and octahedral sheets (Tazaki, 1982; Noro, 1986; Bailey, 1989). The elemental compositions for the three distinct types of crystals observed in the present study were determined by AEM. Histograms showing the frequency distribution of elemental compositions for particles with distinct morphologies are shown in Figure 18. Iron content is

https://doi.org/10.1346/CCMN.1992.0400211 Published online by Cambridge University Press

expressed as FeO as the oxidation states of the Fe is unknown. The data for SiO_2, Al_2O_3 and FeO are not distributed normally. No systematic differences in composition occur between halloysite tubes and laths or kaolinite plates (Table 1). Similarly, no compositional differences were observed between kaolin crystals with different morphologies by Banfield and Eggleton (1990). The iron content of halloysite is consistent with reported values for tubular halloysites but is not systematically different from average values for laths and kaolinite crystals. Tazaki (1982) used AEM to analyze morphologically-distinct crystals in 15 halloysite samples. The samples dominated by crinkly films contained high amounts of FeO (3–15%) while those that were dominantly tubular contained only "traces" of FeO (<1%). Platy halloysites rich in iron have also been reported by other workers (Kunze and Bradley,

←

Figure 13. High magnification transmission electron micrograph of cross sections of halloysite tubes. Tubes show a folded morphology and are joined together by material which may be remnants of the common plate from which the tubes originated.

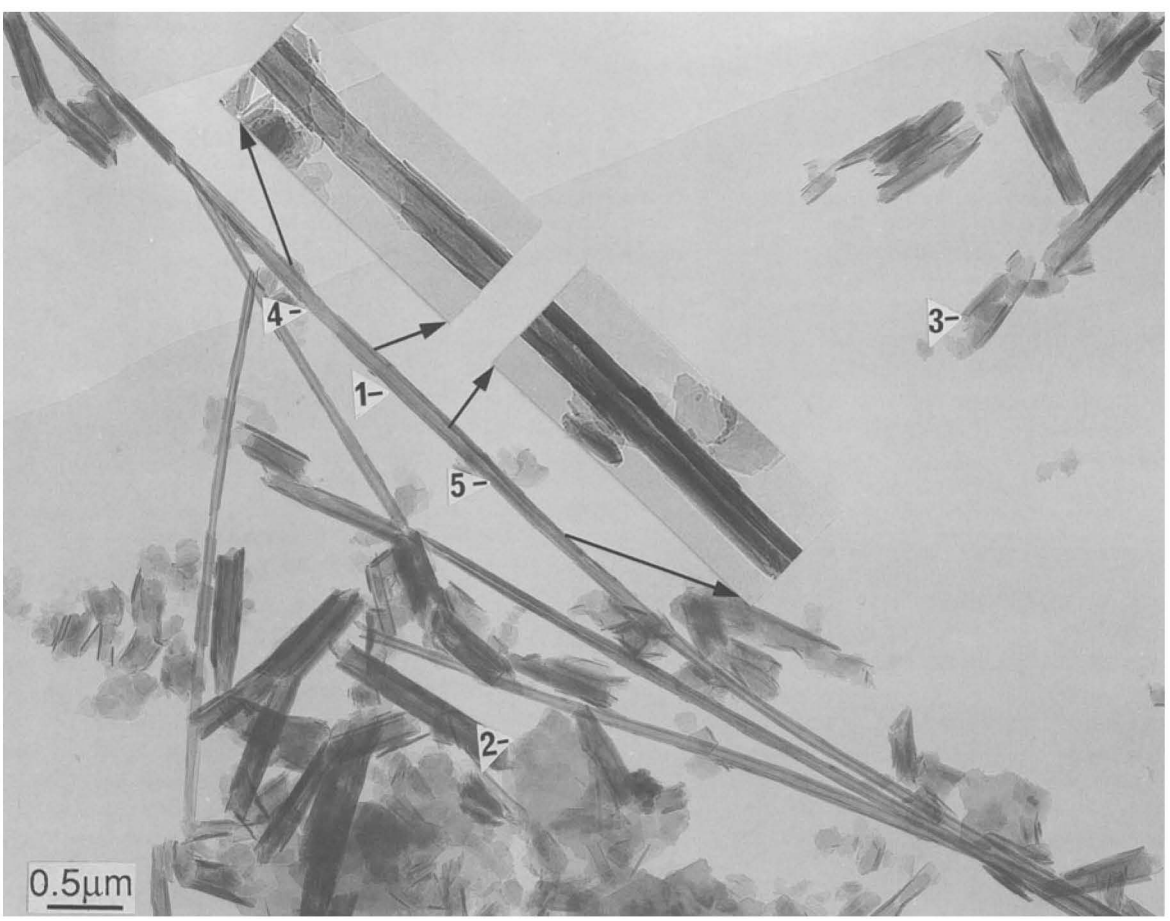

https://doi.org/10.1346/CCMN.1992.0400211 Published online by Cambridge University Press

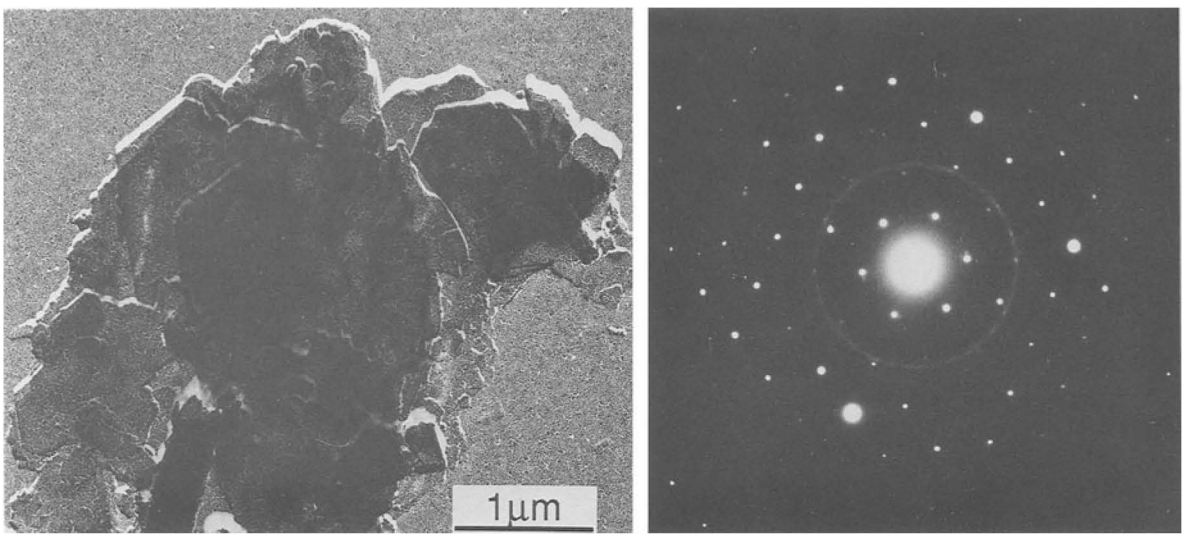

Figure 15. Transmission electron micrograph and characteristic single crystal pseudohexagonal SAED pattern of a complex, kaolinite plate in the dispersed sample.

1964; Wada and Mizota, 1982; Noro, 1986; Delvaux *et al.*, 1990). All the samples analyzed by Tazaki (1982) contained some crystals of each type of morphology, varying from long tubes to thin films. The chemical composition of crystals within a sample did not always vary with differences in morphology, which is consistent with our observations. For instance, the SiO_2/Al_2O_3 ratio for halloysite tubes that contained only traces of iron ranged from 1.17 to 2.22 (Tazaki, 1982). It appears that, besides chemical composition, physical factors may also control the morphology of halloysite (i.e., degree of rolling). In the present instance, where there are no systematic differences in chemical composition, these factors may be the major cause of variation in the morphology of halloysite crystals within a sample.

The cation exchange capacity (CEC) of the clay fraction of the bulk sample was 5.1 meq/100 g, which is small and typical of kaolin group minerals. A CEC value of 2 meq/100 g for tubular halloysite was reported by Noro (1986). However some iron-rich platy halloysites have CEC value ranging from 20 to 60 meq/100 g (Kunze and Bradley, 1964; Wada and Mizota, 1982; Noro, 1986; Delvaux *et al.*, 1990). High values are probably due to octahedral substitution of Al by Fe^{2+} (Tazaki, 1982) or to interstratification by smectite layers in halloysite (Quantin *et al.*, 1984; Delvaux *et al.*, 1990). The clay fraction of this specimen consists of a mixture of kaolinite and halloysite so that the

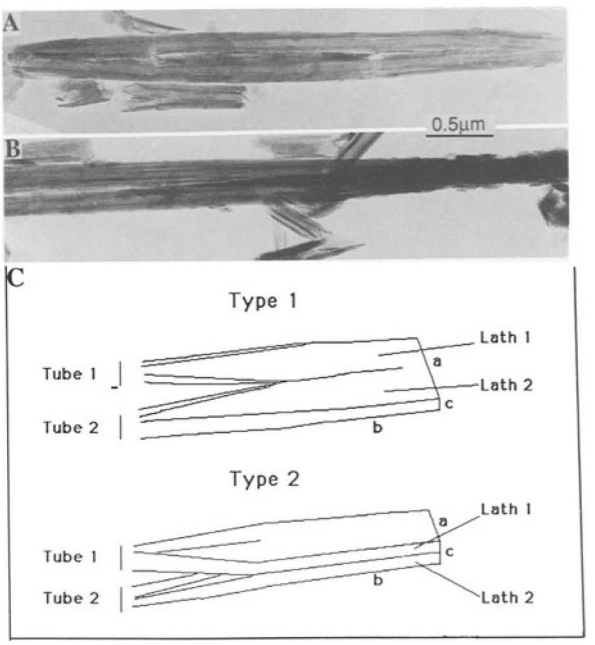

Figure 16. Transmission electron micrograph of the dispersed sample showing two types of twinning of halloysite tubes/laths. (A) The tubes/laths are joined side by side due to cleavage of parent lath approximately perpendicular to (001). (B) The two tubes have exfoliated from one lath/tube due to cleavage along (001). (C) An illustration of these two mechanisms for the formation of halloysite tubes.

←

Figure 14. Transmission electron micrograph of a dispersed sample showing halloysite tubes up to 10 μm in length (1), kaolinite plates (2), and partially rolled laths (3). Some single halloysite crystals exhibit varying degrees of rolling along their lengths ranging from flat to perfectly tubular. The platy and tubular regions of a tube marked (4) and (5) are shown in enlargements.

https://doi.org/10.1346/CCMN.1992.0400211 Published online by Cambridge University Press

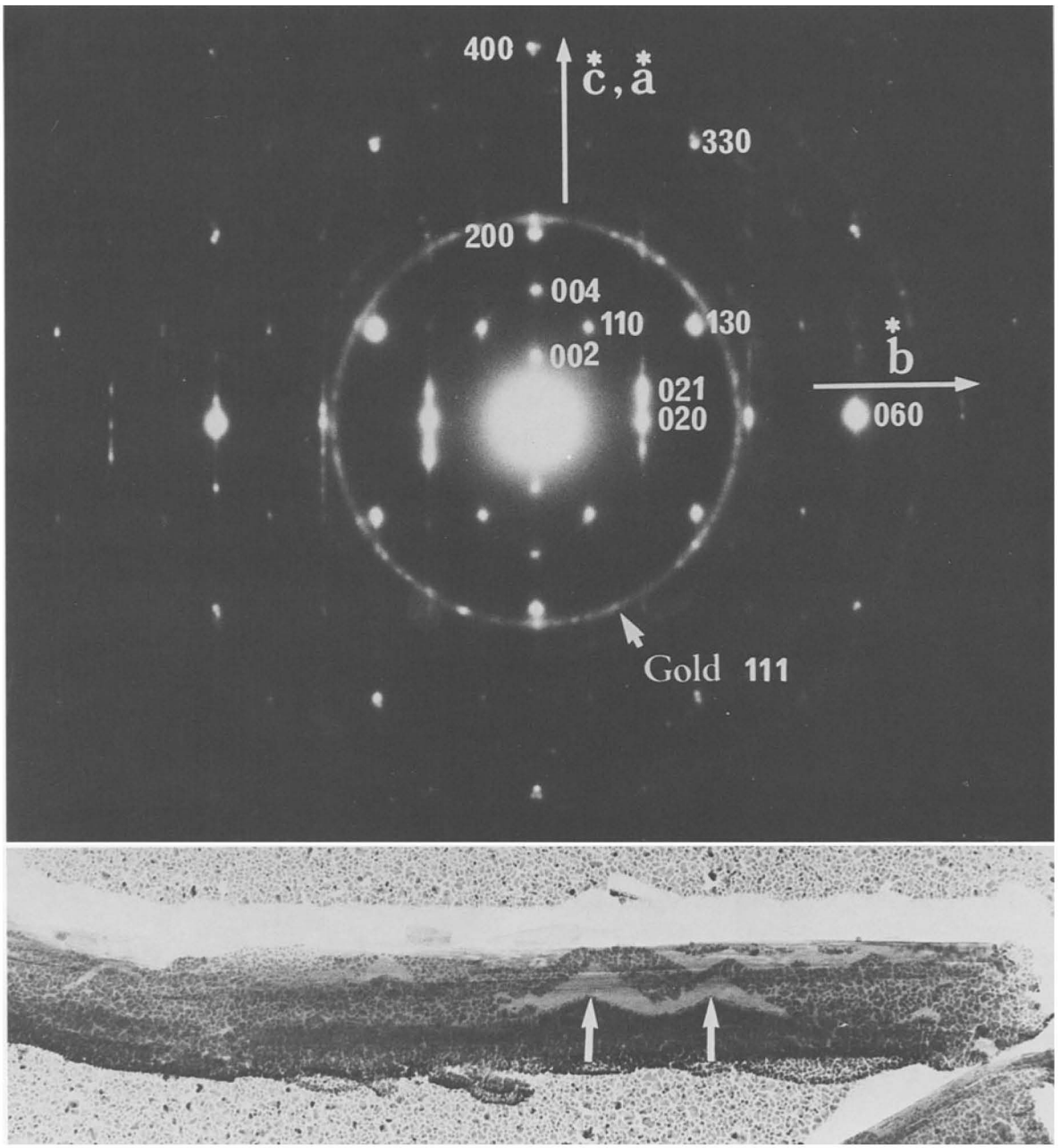

Figure 17. A typical SAED pattern of a gold shadowed halloysite tube indexed on the basis of a two layer (c = 14 Å) structure and showing that elongation is along the direction of the b axis. Angular terminations of crystal faces on the tube are revealed by the shadows on the tube indicated by white arrows.

measured values of CEC for the clay fraction is a composite value for the two minerals.

In order to assess whether there was any relationship between crystal morphology and CEC it is necessary to measure the CEC of individual crystals. The CEC of the individual crystals of halloysite and kaolinite was determined by AEM analysis of Ba-saturated samples. The values of CEC for laths (average value, 2.8 meq/100 g) and kaolinite plates (1.9 meq/100 g) determined by AEM were very variable (Figure 18) and average values were almost identical for the two minerals (Table 1). Halloysite tubes had a higher mean value of CEC (4.5 meq/100 g), but the high variability of the data prevents this result from being statistically significant (p = 0.01). Plots of CEC versus Fe- and Al-content of crystals of kaolinite and halloysite are

https://doi.org/10.1346/CCMN.1992.0400211 Published online by Cambridge University Press

Table 1. Average values of elemental composition and CEC for single crystals of various morphologies in a Ba-saturated sample.

	Halloysite n = 19		Laths n = 11		Kaolinite n = 19	
% Oxide	wt. %	σ	wt. %	σ	wt. %	σ
Al_2O_3	43.94	1.22	43.57	0.73	43.56	1.57
SiO_2	54.99	0.86	55.72	0.61	55.52	1.25
BaO	0.35	0.19	0.21	0.15	0.15	0.17
FeO[1]	0.60	0.38	0.35	0.12	0.74	0.29
CEC (meq/100 g)	4.5	2.5	2.8	1.9	1.9	2.1

[1] Fe expressed as FeO.

shown in Figure 19. Although there is a considerable scatter to the data it appears that CEC may increase with increasing Fe content and decreasing Al content. Thus, CEC may be due to substitution of Fe^{2+} for Al in the octahedral sheet, but this hypothesis would need to be investigated further using Mössbauer and other techniques. The mean values of CEC of individual crystals determined by AEM are similar but smaller than the value for bulk clay. This may be partly due to the fact that the AEM analysis was made on the larger crystals present in the dispersed sample; small crystals may have a higher CEC.

DISCUSSION

The unusual length, parallel orientation, and morphology of halloysite tubes in our material appear to be a consequence of development within a kaolin pseudomorph after mica. It cannot be established if, at the time of crystallization, the kaolinite plates contained the stresses that eventually caused them to fracture and fold, or if the stresses developed subsequently, perhaps on dehydration. The current theories (Bates *et al.*, 1950; Radoslovich, 1963b; Bailey, 1989) explaining the origin of stress and consequent curved morphology of halloysite consider that the stress is inherent in the kaolin structure and that a tubular morphology in the case of halloysite is adopted at the time of crystallization to minimize stress. The kaolinite plates in pseudomorphs after mica crystals may have been stressed due to the lateral misfit of octahedral and tetrahedral sheets as they developed by epitactic/topotactic alteration of mica to kaolinite. Rolling/folding of plates into tubes could not occur due to the restricted volume available within the pseudomorphs and the large lateral size of the plates. Assuming that all the aluminum is retained during weathering, a unit volume of muscovite would weather to almost exactly the same volume of platy hydrated kaolin, leaving no free space for curving to occur. The plates could fracture and curve only when the pseudomorph exfoliated into smaller units. Another consideration is that curving may have occurred after partial dehydration of a 10-Å layer to a spacing of 8.6 or 7.9 Å (Costanzo and Giese, 1985). This would have provided free space for limited curving to occur while interlayer H-bonding was still weak due to the presence of water. The presence of even a few interlayer water molecules can disrupt the hydrogen bonding across the interlayer volume (Giese, 1988). It has been demonstrated by several workers using various techniques (Kohyama *et al.*, 1978; Churchman *et al.*, 1972; Costanzo and Giese, 1985) that halloysite (10 Å) loses interlayer water in steps rather than passing straight from a 10-Å to 7-Å form. While it was constrained in a tightly-packed planar form within the pseudomorph, the platy form may have compensated for the misfit of the lateral dimensions of octahedral and tetrahedral sheets by tetrahedral rotation. When space became available due to partial dehydration and/or exfoliation, curving of the lath-shaped fragments of the halloysite sheets took place and tetrahedral rotation

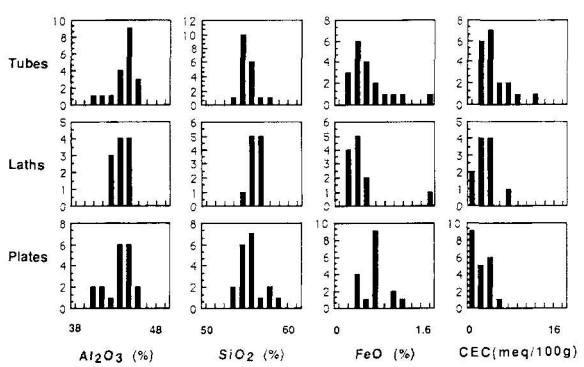

Figure 18. Histograms showing the variation in elemental composition and CEC of single crystals for the three distinct morphological classes of crystals as determined by AEM.

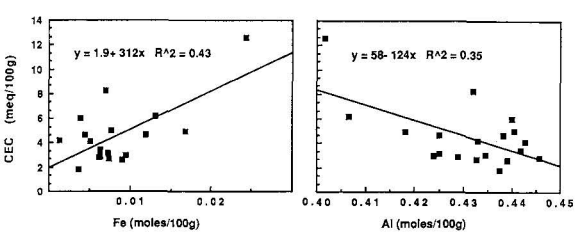

Figure 19. Plots of CEC versus Fe and Al contents for single crystals of kaolinite and halloysite showing that CEC may increase as Fe increases and Al decreases.

https://doi.org/10.1346/CCMN.1992.0400211 Published online by Cambridge University Press

decreased. Thus, the alternative mechanism to correct misfit (i.e., rolling) began to operate and as the curvature increased tetrahedral sheets were able to assume their ideal configuration.

Bailey (1989) hypothesized that exchangeable cations in halloysite are adsorbed adjacent to the tetrahedral side of the interlayer space, due to substitution of Al for Si in the tetrahedral sheet. The exchangeable cations provide the driving force for the introduction of water into the interlayer space. This water, together with cations seated in the hexagonal cavities of the tetrahedral sheet, restricts rotation of tetrahedra (Radoslovich, 1963b), which acts to reduce the dimensions of tetrahedral sheets to minimize misfit. The CEC and (Al + Fe) content of the tubular halloysite described in this investigation are similar to values for the lath-like and platy crystals (Table 1), which may not be consistent with Bailey's (1989) hypothesis that interlayer charge provides the driving force for introduction of water in interlayer space.

ACKNOWLEDGMENTS

We are grateful to B. J. Griffin, T. M. Armitage, and the staff of the Electron Microscopy Center of the University of Western Australia for their assistance. We thank the Editor and S. W. Bailey for their helpful comments. B.S. gratefully acknowledges the Commonwealth Scholarship provided by the Australian International Development Aid Bureau.

REFERENCES

Ahn, J. H. and Peacor, D. R. (1987) Kaolinization of biotite: TEM data and implications for an alteration mechanism: *Amer. Mineral.* **72,** 353–356.

Anand, R. R., Gilkes, R. J., Armitage, T. M., and Hillyer, J. W. (1985) Feldspar weathering in a lateritic saprolite: *Clays & Clay Minerals* **33,** 31–43.

Bailey, S. W. (1989) Halloysite—A critical assessment: in *Proc. Int. Clay Conf., Strasbourg, France,* V. C. Farmer and Y. Tardy, eds., Sci. Géol., Mém. **86,** 89–98.

Banfield, J. F. and Eggleton, R. A. (1988) Transmission electron microscope study of biotite weathering: *Clays & Clay Minerals* **36,** 47–60.

Banfield, J. F. and Eggleton, R. A. (1990) Analytical transmission electron microscope studies of plagioclase, muscovite, and K-feldspar weathering: *Clays & Clay Minerals* **38,** 77–89.

Bates, T. F., Hildebrand, F. A., and Swineford, A. (1950) Morphology and structure of endellite and halloysite: *Amer. Mineral.* **6,** 237–248.

Bates, T. F. (1971) The kaolin minerals: in *The Electron-optical Investigation of Clays,* J. A. Gard, ed., Mineral. Soc., London, 109–157.

Brindley, G. W. and Comer, J. J. (1956) The structure and morphology of a kaolin clay from Les Eyzies (France): *Clays & Clay Minerals,* Natl. Acad. Sci.–Natl. Res. Council Publ. **456,** 61–66.

Chukhrov, F. V. and Zvyagin, B. B. (1966) Halloysite, a crystallochemically and mineralogically distinct species: *Proc. Int. Clay Conf., Jerusalem,* Vol. 1, L. Heller and A. Weiss, eds. Israel Prog. Sci. Transl., Jerusalem, 11–25.

Churchman, G. J., Aldridge, L. P., and Carr, R. M. (1972) The relationship between the hydrated and dehydrated states of an halloysite: *Clays & Clay Minerals* **20,** 241–246.

Churchman, G. J. and Gilkes, R. J. (1989) Recognition of intermediates in the possible transformation of halloysite to kaolinite in weathering profiles: *Clay Miner.* **24,** 579–590.

Churchman, G. J., Whitton, J. S., Claridge, G. G. C., and Theng, B. K. G. (1984) Intercalation method using formamide for differentiating halloysite from kaolinite: *Clays & Clay Minerals* **32,** 241–248.

Costanzo, P. M. and Giese, R. F., Jr. (1985) Dehydration of synthetic hydrated kaolinite: A model for dehydration of halloysite (10 Å): *Clays & Clay Minerals* **33,** 415–423.

Delvaux, B., Herbillon, A. J., Vielvoye, L., and Mestdagh, M. M. (1990) Surface properties and clay mineralogy of hydrated halloysitic soil clays. II Evidence for the presence of halloysite/smectite (H/Sm) mixed-layer clays: *Clay Miner.* **25,** 141–160.

Dixon, J. B. (1989) Kaolin and serpentine group minerals: in *Minerals in Soil Environments,* J. B. Dixon and S. B. Weed, eds., Soil Sci. Soc. America, Madison, Wisconsin, 468–519.

Dixon, J. B. and McKee, T. R. (1974) Internal and external morphology of tubular and spheroidal halloysite particles: *Clays & Clay Minerals* **22,** 127–137.

Eswaran, H. and Bin, W. C. (1978) A study of deep weathering profile on granite in peninsular Malaysia: II. Mineralogy of the clay, silt, and sand fractions: *Soil Sci. Soc. Am. J.* **42,** 149–158.

Giese, R. F., Jr. (1988) Kaolin minerals: Structures and stabilities. Chap. 3: in *Hydrous Phyllosilicates (Exclusive of Micas),* S. W. Bailey, ed., MSA Reviews in Mineralogy **19,** 29–66.

Gilkes, R. J. and Suddhiprakarn, A. (1979) Biotite alteration in deeply weathered granite. II The oriented growth of secondary minerals: *Clays & Clay Minerals* **27,** 361–367.

Gilkes, R. J., Anand, R. R., and Suddhiprakarn, A. (1986) How the microfabric of soils may be influenced by the structure and chemical composition of parent minerals: in *Trans. Int. Soil Sci. Conf. Hamburg* **6,** 1093–1106.

Gilkes, R. J., Scholz, A., and Dimmock, G. M. (1973) Lateritic deep weathering of granite: *J. Soil Sci.* **24,** 523–536.

Honjo, G. and Mihama, K. (1954) A study of clay minerals by electron diffraction diagrams due to individual crystallites: *Acta Cryst.* **7,** 511–513.

Honjo, G., Kitamura, N., and Mihama, K. (1954) A study of clay minerals by means of single crystal electron diffraction diagrams—The structure of tubular kaolin: *Clay Minerals Bull.* **4,** 133–141.

Hope, E. W. and Kittrick, J. A. (1964) Surface tension and morphology of halloysite: *Amer. Mineral.* **49,** 859–866.

Keller, W. D. (1978) Classification of kaolins exemplified by their textures in scan electron micrographs: *Clays & Clay Minerals* **26,** 1–20.

Kirkman, J. H. (1981) Morphology and structure of halloysite in New Zealand tephras: *Clays & Clay Minerals* **29,** 1–9.

Kohyama, N., Fukushima, K., and Fukami, A. (1978) Observation of the hydrated form of tubular halloysite by an electron microscope equipped with an environmental cell: *Clays & Clay Minerals* **26,** 25–40.

Kunze, G. W. and Bradley, W. F. (1964) Occurrence of a tabular halloysite in a Texas soil: *Clays & Clay Minerals* **12,** 523–527.

McCrea, A. F., Anand, R. R., and Gilkes, R. J. (1990) Mineralogical and physical properties of lateritic pallid zone materials developed from granite and dolerite: *Geoderma* **47,** 33–57.

Millot, G. (1970) *Geology of Clays:* Springer-Verlag, Berlin, 429 pp.

Noro, H. (1986) Hexagonal platy halloysite in an altered tuff bed, Komaki City, Aichi Prefecture, central Japan: *Clay Miner.* **21,** 401–415.

Quantin, P., Herbillon, A. J., Janot, C., and Sieffermann, G. (1984) L'halloysite blanche riche en fer de Vate (Vanuatu)—Hypothese d'un edifice interstratifie halloysite-hisingerite: *Clay Miner.* **19,** 629–643.

Radoslovich, E. W. (1963a) Cell dimension studies on layer lattice silicates: A summary: *Clays & Clay Minerals* **11,** 225–228.

Radoslovich, E. W. (1963b) The cell dimensions and symmetry of layer-lattice silicate. VI. Serpentine and kaolin morphology: *Amer. Mineral.* **48,** 368–378.

Robertson, I. D. M. and Eggleton, R. A. (1991) Weathering of granitic muscovite to kaolinite and halloysite and plagioclase-derived kaolinite to halloysite: *Clays & Clay Minerals* **39,** 113–126.

Ross, G. J., Kodama, H., Wang, C., Gray, J. T., and Lafreniere, L. B. (1983) Halloysite from a strongly weathered soil at Mont Jacques Cartier, Quebec: *Soil Sci. Soc. Am. J.* **47,** 327–332.

Souza Santos, P. De. (1966) Mineralogical studies of kaolinite-halloysite clays: Part III. A fibrous kaolin mineral from Piedade, Sao Paulo, Brazil: *Amer. Mineral.* **50,** 619–627.

Spurr, A. R. (1969) A low viscosity epoxy resin: Embedding medium for electron microscopy: *J. Ultrastruct. Res.* **26,** 31–43.

Tazaki, K. (1982) Analytical electron microscopic studies of halloysite formation—Morphology and composition in halloysite: in *Proc. 7th Int. Clay Conf., Italy,* H. van Olphen and F. Veniale, eds., Elsevier, Amsterdam, 573–584.

Towe, K. M. and Hamilton, G. H. (1968) Ultramicrotome-induced deformation artifacts in densely calcified material: *J. Ultrastruct. Res.* **22,** 274–281.

Wada, S. and Mizota, C. (1982) Iron-rich halloysite (10 Å) with crumpled lamellar morphology from Hokkaido, Japan: *Clays & Clay Minerals* **30,** 315–317.

Williams, I. R. (1975) South Western Province: in *Geology of Western Australia,* West. Austral. Geol. Surv., Mem. **2,** Geol. Surv. W. Australia 65–69.

(Received 16 May 1991; accepted 4 December 1991; Ms. 2103)